PHYSICAL REVIEW B **95**, 060403(R) (2017)

First-principles spin-transfer torque in CuMnAs|GaP|CuMnAs junctions

Maria Stamenova,[1,*] Razie Mohebbi,[2] Jamileh Seyed-Yazdi,[2] Ivan Rungger,[3] and Stefano Sanvito[1]
[1]*School of Physics, AMBER and CRANN Institute, Trinity College, Dublin 2, Ireland*
[2]*Department of Physics, Vali-e-Asr University of Rafsanjan, Rafsanjan, Iran*
[3]*National Physical Laboratory, Teddington TW11 0LW, United Kingdom*
(Received 29 November 2016; revised manuscript received 13 January 2017; published 7 February 2017)

We demonstrate that an all-antiferromagnetic tunnel junction with current perpendicular to the plane geometry can be used as an efficient spintronic device with potential high-frequency operation. By using state-of-the-art density functional theory combined with quantum transport, we show that the Néel vector of the electrodes can be manipulated by spin-transfer torque. This is staggered over the two different magnetic sublattices and can generate dynamics and switching. At the same time the different magnetization states of the junction can be read by standard tunneling magnetoresistance. Calculations are performed for CuMnAs|GaP|CuMnAs junctions with different surface terminations between the antiferromagnetic CuMnAs electrodes and the insulating GaP spacer. We find that the torque remains staggered regardless of the termination, while the magnetoresistance depends on the microscopic details of the interface.

DOI: 10.1103/PhysRevB.95.060403

Antiferromagnetic (AF) materials are magnetically ordered compounds where two or more spin sublattices compensate each other, resulting in a vanishing macroscopic magnetization. As a consequence, an antiferromagnet does not produce stray field, and closely separated AF nanostructures are not magnetostatically coupled. In addition, the typical time scale for the dynamics of the antiferromagnetic order parameter, the Néel vector, is set by the AF resonance frequency, which is typically much larger than that of a ferromagnet, and may approach the THz range [1]. It is then not surprising that antiferromagnets have recently received considerable attention as a materials platform for magnetic data storage, logic, and high-frequency applications [2]. One limitation of the AF materials class is the fact that most antiferromagnets are insulators, while often spintronics devices require driving currents through the structure.

Recently, metallic CuMnAs has been proposed as a good candidate for AF spintronics applications [3]. Tetragonal CuMnAs is antiferromagnetic at room temperature and can be grown epitaxially on GaP. Furthermore, it has been shown that one can manipulate the Néel vector of CuMnAs thin films by electric current pulses [4]. This is explained as the result of atomically staggered spin-orbit torques (SOTs),[1] which accompany the current flow in antiferromagnets where the global inversion symmetry is broken due to the presence of two spin sublattices forming inversion partners [5]. The reported Néel temperature of CuMnAs is (480 ± 5) K [6], while the lattice parameters of bulk tetragonal CuMnAs are $a = b = 3.820$ Å and $c = 6.318$ Å. According to density functional theory (DFT) calculations, CuMnAs in its AF ground state is metallic, but it has a rather low density of states at the Fermi level [3]. Here, we investigate whether such a unique AF metal can be used in standard magnetic tunnel junctions (MTJs) and demonstrate that these can be written by spin-transfer torques (STTs) and read by standard tunnel magnetoresistance (TMR).

We consider the two CuMnAs|GaP|CuMnAs stacks depicted in Fig. 1. These are built along the CuMnAs [001] direction with the GaP spacer taking a zincblende structure. In both cases CuMnAs is terminated at the Cu plane and the two electrodes are atomically mirror symmetric with respect to the central $(x$-$y)$ plane in the junction. The spacer can then be terminated either at the Ga plane (GPG junction) or at the P one (PGP). In both cases the total number of atoms in the junction supercell is the same, 49 atoms. The different terminations of the spacer result in interfaces where P binds on top to the Cu surface in PGP, while Ga is in hollow site in GPG [3,4] (see also the Supplemental Material (SM) [7]).

The local spin-density approximation (LSDA) is able to reproduce the experimentally observed AF structure of CuMnAs [3] in its tetragonal phase for the experimental lattice parameters. Both the GPG and the PGP junctions consist of three CuMnAs unit cells on each side of a 3-unit-cell-long GaP spacer region. In addition, there is an extra Ga/P layer at one of the interfaces which makes the junctions more symmetric. The whole stacks are relaxed in the z direction within LSDA using periodic boundary conditions in all directions with the SIESTA [8] code. After the geometry optimization, the z coordinates of all atoms in both junctions are further symmetrized with respect to the junction center, with the intention to suppress additional geometry-driven asymmetry effects to the transport properties. In the final geometries, the lead atoms map ideally onto the same species upon reflection in the $(x$-$y)$ plane through the central atom, and the same is true also for the z coordinates of the spacer atoms, but their corresponding x and y coordinates do not match as the zincblende lattice lacks such a symmetry. In the GPG junction the Cu-Ga distance along the z axis is 1.75 Å for both interfaces, while in the PGP junction the Cu-P distance is 2.16 Å for both interfaces. The total length of the junction is 54.5 Å for the GPG and 54.9 Å for the PGP.

Electron transport through the junctions is described by the Keldysh nonequilibrium Green's function (NEGF) method as implemented in the SMEAGOL code [9–11]. We consider a steady-state formulation of the STT analogous to that described in Ref. [12]. The key points of our STT implementation

*stamenom@tcd.ie
[1]These are also referred to as Néel-order spin-orbit torque fields [5].

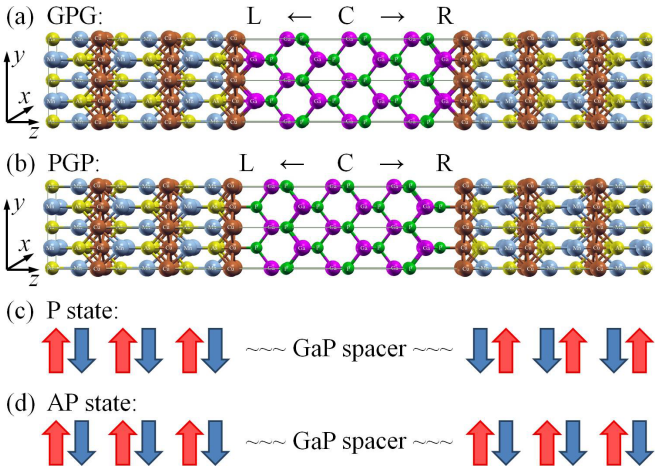

FIG. 1. Atomistic depictions of the two CuMnAs|GaP|CuMnAs junctions studied, differing by their spacer terminations: (a) Ga-terminated structure (labeled as GPG) and (b) P-terminated structure (PGP). The position of the central atomic layer is marked by "C" and the labels "L" and "R" stand for the left- and right-hand-side half of the junction. (c) and (d) show diagrams of the two spin configurations considered, the arrows indicating the direction of the spin of all Mn atoms in a corresponding vertical layer above. We define a parallel (P) and antiparallel (AP) spin state of the junction, respectively, based on the orientation of the two innermost Mn planes (i.e., in the AP case the R-lead order parameter is rotated by 180° with respect to the P state). The coordinate system is chosen such that the z axis is along the transport direction, while the Néel vectors of the leads lie in the (x-y) plane and the spin quantization axis is along y.

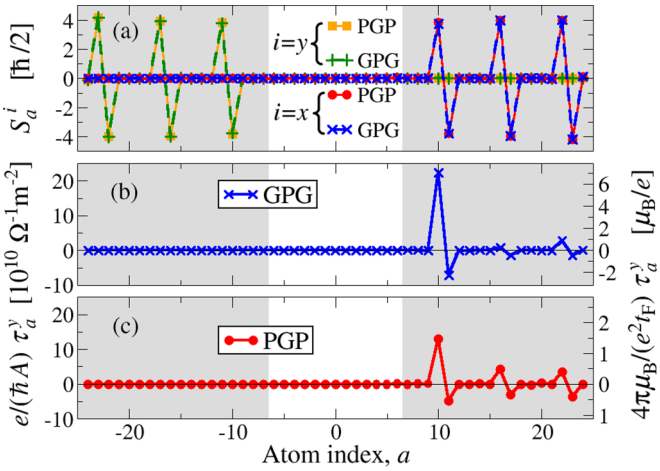

FIG. 2. Ground state observables atomically projected along the z direction in each of the two junctions for the 90° alignment of the lead order parameters: (a) The x and y components of the local spin moments and (b), (c) the spin-transfer torkance per unit area (for both junctions $A = 14.59$ Å^2) for GPG and PGP, respectively. The torkance is also converted to torque per current in units of μ_B/e using the corresponding Fermi-level transmission coefficients [7] computed for the 90° alignment $t_F = 2.4 \times 10^{-4}$ for GPG and $t_F = 6.7 \times 10^{-4}$ for PGP.

are described in the SM [7]. The STT at each atomic site a carrying a spin $\mathbf{S}_a$ is defined as

$$\mathbf{T}_a = \frac{1}{2}\mathrm{Re}\sum_{i\in a}\sum_{j}\mathbf{\Delta}_{ij}\times\boldsymbol{\sigma}_{\mathrm{tr},ji}, \quad (1)$$

where $\mathbf{\Delta}_{ij}$ is a matrix element of the exchange-correlation potential (i,j designate orbitals of the local atomic basis) and $\boldsymbol{\sigma}_{\mathrm{tr},ij}$ is the nonequilibrium (transport) matrix element of the spin-traced density matrix [7]. The latter matrix elements are finite in the case of spin noncollinearity in the open-boundary system. In the limit of a small applied external bias voltage we evaluate the linear-response STT, i.e., the spin-transfer *torkance* (STTk), as

$$\boldsymbol{\tau}_a = \mathbf{T}_a/\delta V = \frac{1}{2}\sum_{i\in a}\sum_{j}\mathbf{\Delta}_{ij}\times\mathrm{Tr}\left[\frac{\partial\rho_{ji}(V)}{\partial V}\boldsymbol{\sigma}\right]_{V=0}, \quad (2)$$

where ρ is the equilibrium density matrix in the NEGF formalism.

We evaluate the atomically resolved SSTk in the right-hand-side lead (RL) for the largest misalignment of 90° between the two lead order parameters, i.e., for the Mn spins in the left-hand-side lead (LL) oriented along the y axis, while the RL spins are rotated by 90° about the z axis starting from the P state, hence the order parameter in RL is now along x [Fig. 2(a)]. The local exchange field $\mathbf{\Delta}_a$ within LSDA shows a very similar staggered distribution (not shown here) and the resulting STTk in the RL is also staggered. STTk is maximal at the very first Mn layer and then decreases in magnitude in the following Mn layers. Despite the limiting size of the MTJ stacks considered here, this provides clear indications of decay but also saturation of the staggered in-plane STTk in the AF lead away from the interface. This behavior of the SSTk is similar to what has been found by first-principles calculations in AF spin valves [13] and attributed to the interference of multiple open channels with different k_z at the Fermi level. It had been previously demonstrated that in the limit of a single open channel, in model AF junctions, the nonequilibrium spin density ($\sigma^z_{\mathrm{tr},a}$) is uniformly distributed in the lead [14], but this picture breaks down in the case of multichannel conductance. Most importantly, the staggered property of the STTk observed in both junctions, which is crucial for the manipulation of the AF order parameter by currents, appears to be a robust property of the AF junctions, and it is weakly affected by the chemistry of the interfaces.

The magnitude of the STTk we find at the interfacial Mn is larger than those obtained in Fe by similar first-principles calculations for Fe|MgO|Fe MTJs in Ref. [15] for a similar thickness of the barrier in terms of monolayers (six in the FeMgOFe case). As a guiding estimate of the critical bias for switching we assume a macrospin approximation [16] for the 3-unit-cell-long part of the right electrode, which gives $V_c = \alpha E_{\mathrm{ani}}/\tau^y$ (note that there are no demagnetizing fields in the case of an AF which reduces the critical bias and current in this case). Considering the sum of the absolute values of the atomic torkances in Fig. 2, which is equal to $36.8 \times 10^{10}\ \Omega^{-1}\,\mathrm{m}^{-2}$ ($33.8 \times 10^{10}\ \Omega^{-1}\,\mathrm{m}^{-2}$) for GPG (PGP), a magnetocrystalline anisotropy energy $E_{\mathrm{ani}} = 0.127$ mV per unit cell [6], and a tentatively large damping constant $\alpha = 0.1$, we obtain a critical bias for switching $V_c = 0.17$ V for GPG and $V_c = 0.19$ V for PGP. This corresponds (assuming constant transmission

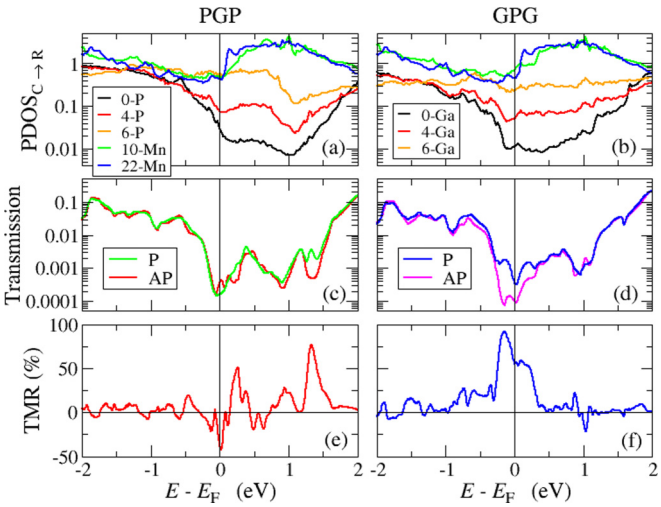

FIG. 3. Electronic and transport properties of the two junctions in the P state: (a), (b) The PDOS of atoms in the (C → R) half of the junction. The atom indexes are the same as in Fig. 2. Note that the black curves correspond to the atom (P or Ga) in the very center of the junctions. (c) and (d) show the spectrum of the total transmission in both the P and AP state, while in (e) and (f) the TMR is defined as TMR $= (t_P - t_{AP})/(t_P + t_{AP})$.

t_F at values used in Fig. 2) to critical currents of $I_c = 1.1 \times 10^{10}$ A/m^2 for GPG and $I_c = 3.3 \times 10^{10}$ A/m^2 for PGP.[2]

Let us now investigate in more detail the electronic and transport properties of each junction in its collinear (P or AP) state. The atomically projected density of states (PDOS) [7] in Figs. 3(a) and 3(b) shows that the phosphorus interface layer in PGP is almost metallized, and there is a progressive reduction of the P-atom PDOS when moving away from the interface for energies between E_F and $E_F + 2$ eV. This range corresponds to the energy gap in the middle of the GaP spacer. The trend is similar for the Ga atoms in GPG, although the junction is clearly more insulating in the middle compared to PGP. The Fermi level in both cases lies within the GaP gap, close to the valence band top, so that transport is via tunneling. As such, the transmission coefficient, $t = t^{\uparrow} + t^{\downarrow}$, is reduced in the energy range of the gap [Figs. 3(c) and 3(d)], and the main features are the same for GPG and PGP, as well as for the P and AP configurations. Importantly, for the GPG junction there is a significant energy interval ± 0.3 eV around E_F, where the P configuration has significantly higher t than the AP one, resulting in the large TMR of 50%–100% [Figs. 3(c) and 3(d)]. In contrast, in the PGP junction the TMR does not display such an extended plateau, but rather shows an oscillating energy dependence, and in the vicinity of E_F there is an abrupt TMR sign reversal when compared to the GPG case. This is followed by an energy range above E_F where TMR > 0 and then another region with significant TMR corresponding to the bottom of the GaP conduction band. Such an oscillatory character of the TMR in the PGP junction suggests that the actual value may be sensitive to the exact details of the atomic interfaces, while for the GPG case it can be expected to be robust.

[2]We approximate the critical current as $I_c = \frac{e^2}{2\pi\hbar} t_F V_c$.

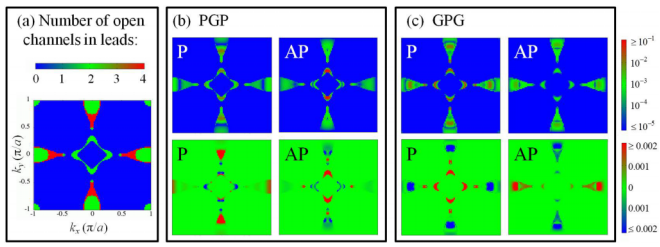

FIG. 4. Contour plots in the two-dimensional (k_x,k_y) BZ orthogonal to the transport direction for various transport quantities. (a) depicts the total number of open channels in the CuMnAs leads; (b) and (c) show the Fermi-level transmission $t(k_x,k_y)$ (top panels) and the spin-polarized transmission $\mathrm{Tr}[\hat{t}(E_F)\hat{\sigma}^z]$ (bottom panels) in the P and AP state and for the PGP and GPG junction, respectively.

For further insight we compare the GPG and PGP transmissions $t_{\mathbf{k}}$ at the Fermi level as a function of the transverse $\mathbf{k}_\perp = (k_x,k_y)$ vector resolved over the entire first Brillouin zone (BZ) (Fig. 4). We note that in both cases there are vast regions of the BZ, where $t_{\mathbf{k}} = 0$ (blue areas in the transmission panels). This is a direct consequence of the low DOS in the CuMnAs electrodes around E_F. In fact, in Fig. 4(a) one can directly observe that the regions of k space with $t_{\mathbf{k}} = 0$ essentially correspond to regions where there are no open scattering channels at E_F. Interestingly, and in contrast to the case of Fe|MgO junctions, this is the case also for the BZ center.

It is also interesting to note that the spin-polarized transmission, defined as $t_{\mathbf{k}}^{\uparrow} - t_{\mathbf{k}}^{\downarrow}$, shows that for different pockets in the BZ, the spin of the current-carrying electrons is opposite. For example, for the GPG junction and P configuration the electrons have up spin for the pockets close to the BZ center, while they have down spin for the pockets at the BZ boundary. In contrast, for the AP configuration the pockets at $k_y = 0$ have up spins, while the ones at $k_x = 0$ have down spins, so that the fourfold rotational symmetry in the $(x$-$y)$ plane is broken. This is due to the fact that the GPG structure breaks this symmetry in the $(x$-$y)$ plane, since the Ga-P bonds at the two interfaces are 90° rotated with respect to each other. The imprint of such geometric asymmetry in the transmission indicates a strong contribution of d orbitals around E_F.

Finally, we look at the Fermi-level PDOS and in particular the spin PDOS (sPDOS), which we define as the difference for spin-up and spin-down PDOS,[3] as a function of the atomic position a starting from the center of the junction (Fig. 5). sPDOS(a) at E_F is staggered on the Mn sites and consistently oppositely polarized to the on-site Mn spin (see Fig. 1). Importantly, there is a notable difference between the two junctions. For both PGP and GPG, the sPDOS(a) curves for the two P-state partitions and for the AP:(C → L) case are identical. However, the remaining different curve AP:(C → R) has a cumulative sPDOS with an opposite sign for the GPG

[3]The PDOS is defined as $N^\sigma(E) = \frac{1}{2\pi}\mathrm{Tr}[A^\sigma(E)\Omega]$, where $A^\sigma(E) = 2\pi \sum_n \delta(E - E_n^\sigma)\psi_n^\sigma \psi_n^{\sigma\dagger}$ is the spectral function for each spin component $\sigma = \uparrow, \downarrow$; Ω is the local basis overlap matrix and ψ_n^σ are the Kohn-Sham (KS) solutions of the open-boundary problem corresponding to eigenvalue E_n^σ.

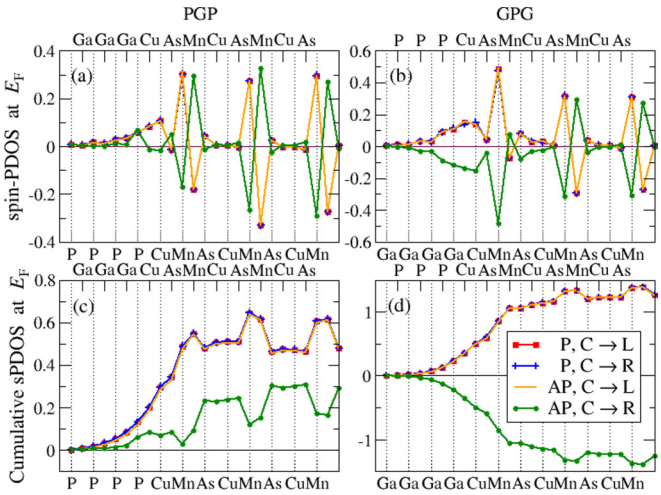

FIG. 5. (a), (b) Fermi-level spin PDOS as a function of atom position in one of the two partitions [(C → L) or (C → R)] for the P and AP spin state of each junction. In (c) and (d) the cumulative spin PDOS is shown, integrated from the center of the junction in all cases. The symbol legend is in (d).

junction and with the same sign for the PGP. Thus in the GPG stack the spin polarization induced inside the spacer around each interface carries the same sign as the Mn atom at the interface, while this is not the case for the PGP junction in the AP state. This suggests that the TMR in the GPG structure resembles the conventional TMR of ferromagnetic junctions as described by the Jullière model [17]. In fact, it can be seen in Fig. 5(d) that the PDOS distributions for majority and minority spins swap as the noncompensated spin polarization reverses in the right-hand-side lead between the P and the AP state.

In the SM [7] we provide a detailed analysis of the $\mathbf{k}_\perp$-dependent sPDOS around E_F, and we show further evidence that, while for the GPG structure the transmission properties are mainly driven by bulklike features, for the PGP they are determined by interface states. The LL and RL interfacial Mn layers (10-Mn in Fig. 3) in the GPG case have large positive Fermi-level spin polarizations for the P state, which are very similar in their $\mathbf{k}_\perp$ dependence and resemble the sPDOS of the bulk Mn atoms. This is not the case for the PGP, where the E_F spin polarizations of 10-Mn and 11-Mn are very different from the bulk-Mn sPDOS structures in the reciprocal space. For both junctions in the AP state the 10-Mn (RL) shows the exact opposite negative spin polarization (from the P state), and only in the next 11-Mn layer the spin polarization is positive. Evidently, the effective tunneling distance for each spin channel for the bulklike states of GPG is therefore increased for the AP configuration compared to the P one, so a smaller conductance for the AP in this case is expected, manifesting itself in the positive TMR [Fig. 3(f)]. In the PGP case the TMR is governed by the symmetries of the interface states and shows a resonant nature.

In conclusion, we have shown that MTJ stacks made solely of antiferromagnets display staggered spin-transfer torques when the current flows in a direction perpendicular to the plane. This fact is little affected by surface termination and strongly suggests that the AF order parameter can be manipulated by currents. Furthermore, such junctions exhibit pronounced magnetoresistance, which is intrinsic of having a global inversion asymmetry in the stacks. We have deliberately suppressed some of the interface-driven structural inversion asymmetry and compared two junctions which defer by their spacer terminations. We have demonstrated that even under such symmetry enhancement the CuMnAs-based junctions show a significant magnetoresistance effect and that a Ga-Cu termination of the CuMnAs|GaP interface particularly improves the TMR robustness. Our work thus demonstrates that all-antiferromagnetic junctions are both readable and writable with an electrical current, and therefore are interesting candidates as high-frequency, high-density memory elements.

This work is supported by Science Foundation Ireland (Grants No. 14/IA/2624 and No. 16/US-C2C/3287) and from the European Union's Horizon2020 programme PETMEM project (Grant No. 688282). We gratefully acknowledge the DJEI/DES/SFI/HEA Irish Centre for High-End Computing (ICHEC) for the provision of computational facilities. Some of the calculations were performed on the Parsons cluster maintained by the Trinity Centre for High Performance Computing and funded through grants from SFI. R.M. gratefully acknowledges a travel grant from the Iranian Ministry of Science and Technology for her visit to Dublin.

[1] J. M. D. Coey, *Magnetism and Magnetic Materials* (Oxford University Press, Oxford, UK, 2009).

[2] T. Jungwirth, X. Martì, P. Wadley, and J. Wunderlich, Nat. Nanotechnol. **11**, 231 (2016).

[3] P. Wadley, V. Novák, R. P. Campion, C. Rinaldi, X. Martì, H. Reichlová, J. Železný, J. Gazquez, M. A. Roldan, M. Varela, D. Khalyavin, S. Langridge, D. Kriegner, F. Máca, J. Mašek, R. Bertacco, V. Holý, A. W. Rushforth, K. W. Edmonds, B. L. Gallagher, C. T. Foxon, J. Wunderlich, and T. Jungwirth, Nat. Commun. **4**, 2322 (2013).

[4] P. Wadley, B. Howells, J. Železný, C. Andrews, V. Hills, R. P. Campion, V. Novák, K. Olejník, F. Maccherozzi, S. S. Dhesi, S. Y. Martin, T. Wagner, J. Wunderlich, F. Freimuth, Y. Mokrousov, J. Kuneš, J. S. Chauhan, M. J. Grzybowski, A. W. Rushforth, K. W. Edmonds, B. L. Gallagher, and T. Jungwirth, Science **351**, 587 (2016).

[5] J. Železný, H. Gao, K. Výborný, J. Zemen, J. Mašek, A. Manchon, J. Wunderlich, J. Sinova, and T. Jungwirth, Phys. Rev. Lett. **113**, 157201 (2014).

[6] P. Wadley, V. Hills, M. R. Shahedkhah, K. W. Edmonds, R. P. Campion, V. Novák, B. Ouladdiaf, D. Khalyavin, S. Langridge, V. Saidl, P. Nemec, A. W. Rushforth, B. L. Gallagher, S. S. Dhesi, F. Maccherozzi, J. Železný, and T. Jungwirth, Sci. Rep. **5**, 17079 (2015).

[7] See Supplemental Material at http://link.aps.org/supplemental/10.1103/PhysRevB.95.060403 for more details on the interfacial geometry and a detailed analysis of the $\mathbf{k}_\perp$-dependent PDOS around E_F.

[8] J. M. Soler, E. Artacho, J. D. Gale, A. Garcìa, J. Junquera, P. Ordejón, and D. Sánchez-Portal, J. Phys.: Condens. Matter **14**, 2745 (2002).
[9] A. R. Rocha, V. M. Garcìa-Suárez, S. Bailey, C. Lambert, J. Ferrer, and S. Sanvito, Phys. Rev. B **73**, 085414 (2006).
[10] A. R. Rocha and S. Sanvito, Phys. Rev. B **70**, 094406 (2004).
[11] I. Rungger and S. Sanvito, Phys. Rev. B **78**, 035407 (2008).
[12] P. M. Haney, D. Waldron, R. A. Duine, A. S. Nũnez, H. Guo, and A. H. MacDonald, Phys. Rev. B **76**, 024404 (2007).
[13] P. M. Haney, D. Waldron, R. A. Duine, A. S. Nũnez, H. Guo, and A. H. MacDonald, Phys. Rev. B **75**, 174428 (2007).
[14] A. S. Núñez, R. A. Duine, P. Haney, and A. H. MacDonald, Phys. Rev. B **73**, 214426 (2006).
[15] C. Heiliger and M. D. Stiles, Phys. Rev. Lett. **100**, 186805 (2008).
[16] D. C. Ralph and M. D. Stiles, J. Magn. Magn. Mater. **320**, 1190 (2008).
[17] M. Jullière, Phys. Lett. A **54**, 225 (1975).